Ocean-Bottom Seismology of Glacial Earthquakes: The Concept, Lessons Learned, and Mind the Sediments

Evgeny A. Podolskiy[a], Yoshio Murai, Naoya Kanna, Shin Sugiyama

[a] ***Corresponding Author:*** *Arctic Research Center / GiCORE, Hokkaido University, Sapporo, Hokkaido 001-0021, Japan, e-mail: evgeniy.podolskiy@gmail.com*

Declaration of Competing Interests:
The authors acknowledge there are no conflicts of interest recorded.

Abstract

Seventy percent of Earth's surface is covered by ocean, where seismic observations are challenging. Seafloor seismology overcame this fundamental difficulty and radically transformed the earth sciences, as it expanded the coverage of seismic networks and revealed otherwise inaccessible features. At the same time, there has been a recent increase in the number of studies on cryoseismology. These have yielded multiple discoveries, but are limited primarily to land/ice-surface receivers. Near ice calving fronts, such surface stations are noisy, primarily due to crevassing and wind, are hazardous to maintain, and can be lost due to iceberg calving. To circumvent these issues, we have applied ocean-bottom seismology to the calving front of a tidewater glacier in northwest Greenland. We present details of this experiment, and describe the technical challenges, noise analysis, and examples of recorded data. This includes tide-modulated seismicity with thousands of icequakes per day and the first near-source (∼200–640 m) underwater record of a major kilometer-scale calving event in Greenland, which generated a glacial earthquake that was detectable ∼420 km away. We also identified a decrease in bottom-water temperature, presumably due to modified water stratification driven by extreme Greenland glacial melting, at the end of July 2019. Importantly, we identify that glacial sediments are the key reason for the anomalously long (∼9.7 h) delay in the sensor release from the fjord seafloor. Our study demonstrates a methodology to undertake innovative, interdisciplinary, near-source studies on glacier basal

sliding, calving, and marine-mammal vocalizations.

INTRODUCTION

One of the fundamental questions in glaciology is what controls glacier basal sliding. In Antarctic and Greenland, the rapid slip of marine-terminating glaciers and ice streams drains interior ice to the ocean (Zoet and Iverson, 2020). This is important for predicting sea-level rise, which may displace up to 180 million people in the 21st century (Bamber et al., 2019). One of the fundamental questions in seismology – what controls tectonic fault slip – is conceptually similar, as it relates to shear zone conditions.

During the past two decades, seismology has been revolutionized by the discovery of slow earthquakes and the recognition that their continuous seismic tremor can be used to monitor otherwise inaccessible faults (Obara, 2002; Rouet-Leduc et al., 2019). In this respect, dense seismic monitoring networks have enabled key discoveries in the earth sciences (Beroza and Ide, 2011). In some regions, seafloor seismic observations were instrumental in detecting non-volcanic tremors (Todd et al., 2018). Polar regions have fast-flowing glaciers, which can be considered analogous to a slow earthquake (Podolskiy and Walter, 2016; Lipovsky and Dunham, 2017). However, testing this analogy is challenging, because seismic stations in polar regions are scarce, dangerous to maintain, moved by ice flow by tens of meters per month, and influenced by noise due to near-surface, tide-modulated icequakes, supraglacial and englacial hydrology, and wind (Podolskiy et al., 2016, 2017; Podolskiy, 2020; Frankinet et al., 2020). Furthermore, for long-term monitoring, the extremely cold temperatures and long polar nights require a large number of batteries, which complicates logistical operations significantly.

In this study, we investigated glacier microseismicity and other terminus processes by seafloor seismology (Fig. 1a). Specifically, we deployed an ocean-bottom seismometer (OBS) near a calving front of grounded Greenlandic glacier. This approach can: (1) protect the seismometer from destruction; (2) provide direct coupling between the sliding base and seismometer; (3) greatly decrease the high-frequency (>5–10 Hz) seismic noise (Webb, 1998); and (4) provide a potentially powerful method to observe the frictional state of the glacier base (e.g., Hudson et al., 2020; Zoet et al., 2020) and monitor other seismic sources in the fjord, including iceberg calving and anthropogenic noise.

Moreover, our approach in not only of interest to glaciologists and seismologists, but also to marine biologists. It has been recognized that it is possible to detect and classify the seasonal occurrence of different species and to track whales with seafloor seismic networks using their vocalizations (Dreo et al., 2019). In Arctic glacier fjords, which contain biologically rich assemblages (Lydersen et al., 2014), animal monitoring is extremely limited and challenging (Podolskiy and Sugiyama, 2020). However, seismometers can detect acoustic vocalizations by some cetaceans (whales). High-frequency sounds of fish, pinnipeds (seals), and delphinids can be recorded with hydrophones. Figure 1b shows examples of seismo-acoustic sources of biological and geophysical origin in Greenland. Integrating hydrophones into the OBS system is relatively easy and less demanding than preparing a standard oceanographic mooring. Moreover, since 1960s passive listening of the ocean soundscape is the foundation of acoustic oceanography, which is an important observational field, both globally (e.g., Munk et al., 1995; Au and Lammers, 2016) and, more recently, in the rapidly changing Arctic and Antarctic (Schulz et al., 2008; Deane et al., 2019; Howe et al., 2019; Dziak et al., 2019; Worcester et al., 2020). Therefore, our methodology has the potential to transform the research approach in one of the most challenging environments on Earth, where there is an urgent need for monitoring (Straneo et al., 2019). For example, the presence and status of endemic Arctic species such as the narwhal are poorly known (Podolskiy and Sugiyama, 2020).

This paper describes our experience of the first deployment of an OBS system at the calving front of a Greenlandic tidewater glacier. Considering that this installation had to be undertaken in previously unexplored circumstances and faced unique difficulties, it provides insights into how to conduct such OBS experiments in the future.

METHODS

Study Site

The OBS deployment site was in northwest Greenland, close to the Qaanaaq settlement (Figs. 2a–b) and next to Bowdoin Glacier (or *Kangerluarsuup Sermia* in Greenlandic; Bjørk et al. (2015)). To understand ice–ocean interactions in Greenland, Bowdoin Glacier and its fjord have been studied intensively since 2013 (e.g., Sugiyama et al., 2015; Podolskiy et al., 2016, 2017; Podolskiy, 2020; Kanna et al., 2018; Ohashi et al., 2020; van Dongen et al., 2021). In particular, it remains the only calving glacier in Greenland where simultaneous passive seismic and geodesic monitoring have been conducted directly on ice close to the calving front, 250 m and less (Podolskiy et al., 2016, 2017). For example, in July 2019, in collaboration with ETH Zürich (VAW), a comprehensive seismic/geodesic monitoring campaign involved at least 15 seismometers and 22 GPS stations (to be published elsewhere). Such background makes Bowdoin Glacier a suitable site for an OBS test. This 3 km wide tidewater glacier slides $\sim 440\,\mathrm{m\,yr^{-1}}$ (Sugiyama et al., 2015). In summer, the glacier slides 1–3 $\mathrm{m\,d^{-1}}$. It terminates in the 250 m deep Bowdoin Fjord and has tidally modulated ice flow. The terminus is nearly floating and can be partially ungrounded along some calving front sections (van Dongen et al., 2021). To our knowledge, no glacial earthquakes associated with the glacier have been detected to date by regional networks. The fjord is visited by narwhals that emit ultrasonic acoustic vocalizations (Podolskiy and Sugiyama, 2020). The OBS deployment location (77.67°N, 68.63°W) was at the center of Bowdoin Fjord, approximately 640 m from the calving front (Fig. 2c). According to boat-based sonar during the deployment, the depth at the OBS drop point was 243 m.

Instrumentation

Our pop-up-type OBS system (Fig. 2d) was used previously in offshore earthquake studies (Shinohara et al., 2008; Machida et al., 2009; Shinohara et al., 2011; Azuma et al., 2012). The system consists of a three-component geophone with a gimbal mechanism (4.5 Hz eigenfrequency; L-28LBH by Katsujima; for details see Appendix A), a recorder digitizing data at 128 sps using a 16-bit A/D converter (Katsujima HDDR2), and an acoustic release system (Kaiyo Denshi STH-10B acoustic transponder connected to a Mitsuya anchor unit). The sensor and recorder are connected to lithium batteries and placed inside a glass sphere under vacuum, which in turn is covered by a protective plastic shell. An autonomous hydrophone with an internal thermometer (SoundTrap ST300 STD by Ocean Instruments) was attached to the shell. The underwater sounds were sampled at 96 kHz and the water temperature was measured every minute at a resolution of 0.1°C. The resulting frequency range of the OBS system is sufficiently broad to cover the vast diversity of possible seismo-acoustic signals in the glacier fjord (Fig. 1b). We present temperature records here, and plan to publish a thorough analysis of the high-frequency hydroacoustic records elsewhere. Finally, for the OBS search and rescue, we utilized a radio beacon (RF-700A1 by Novatech).

Manual Deployment

OBS operations usually require heavily equipped and complex research vessels with technicians and a davit to deploy, find, and retrieve instruments (e.g., Russel et al., 2019). In our study, the logistics were uniquely challenging. Due to the lack of a port and a vessel with a davit in Qaanaaq, preassembled OBS components were taken one-by-one using a rubber boat from the coast to another small (<1.5 t) boat. After arrival at Bowdoin Fjord, the final OBS assembly was undertaken in a boat anchored in Falcon Bay, which is sheltered from any possible calving events and ice-generated tsunamis (Minowa et al., 2019).

For manual OBS deployment, two boats stopped briefly near the calving front at a safe distance, which would have allowed the boats to flee if necessary. The operation was completed within 10 min, in order to minimize exposure to possible calving events.

After removal of the safety bolts that rigidly fix the lower anchor frame

($\sim$40 kg) to the OBS ($\sim$40 kg), two thin steel necks are the only connectors, which are cut at the OBS release and have to be handled with care to remain intact (Fig. 2d). To avoid putting any pressure onto the anchor frame during deployment, the system was lifted with a metal pole that passed through the upper hinge and was held at both ends by 2×2 people. After placing the pole carrying the OBS between the two boats and lowering it gently, the upper hinge was cut, which dropped the instrument gently into the water.

We note, that in more difficult ice conditions, a similar OBS drop could be conducted using a helicopter (Fig. B1), as we have previously done in offshore Hokkaido (i.e., using a winch to lower the instrument 30–40 m though a hatch). This could not be organized in the summer of 2019 due to the lack of an appropriate helicopter. Bottom lander deployments using remotely operated vehicles (ROVs) near a calving front were attempted recently in Alaska (Nash et al., 2020). Unfortunately, there is as yet no adequate technology for doing this with OBSs.

Data and Analysis

Seismic data were stored initially in a standard Japanese seismic format (i.e., "win"). Data were converted to SAC as velocity using the "win2sac" program of the University of Tokyo. For some results described below, MSEED seismic data from the nearest permanent GLISN stations (Clinton et al., 2014) TULEG and NEEM (76.53°N, 68.82°W, 38 m a.s.l.; 77.44°N, 51.07°W, 2513 m a.s.l., respectively) were downloaded as counts from the IRIS open-access depository and converted to velocity using the associated metadata. In our analysis, we used vertical component seismic traces. Tide data collected 125 km away at Pituffik station (Thule; 76.54°N, 68.86°W) were obtained from the Global Sea Level Observing System network. From the previous analyses of tide data we collected near the calving front of Bowdoin Glacier, it is known that there is no phase and amplitude difference which could affect our interpretations (Podolskiy et al., 2016; Minowa et al., 2019).

The output frequency of the micro-crystal controlling the time may deviate depending on the temperature, and lead to the well-known OBS problem of internal clock drift. Due to logistical difficulties at deployment and retrieval, the internal OBS clock was compared only with watches synchronized to GPS time by taking photographs of the OBS PC interface and watches. This yielded an accuracy of approximately ± 1 s. From the internal clock initiation on July 21 until the final check on August 9, the OBS clock was ahead of the watches by 7 s. This implies that for the period of record on the fjord floor, the time stamp departed gradually from UTC-time and led to seismic arrivals being delayed for up to 6 s at the time of release. We corrected for this "time-stretching" assuming a linear drift. A more precise time correction is out of the scope of this paper, given the associated uncertainty is of little importance for the results discussed below. However, in a follow-up study, we intend to reconstruct the absolute time by cross-correlating waveforms with surface stations running in parallel to this experiment on rock and glacier surfaces (e.g., Hable et al., 2018).

The relative variation in the number of seismic events was detected using the conventional short-time-average through the long-time-average (STA/LTA) algorithm, with parameters similar to those used in a previous study (Podolskiy et al., 2016). The STA window was 0.2 s, the LTA window was 5 s, the threshold for declaring an event was set to six, and the threshold for declaring the end of the event was set to 0.5. The number of seismic detections was counted within 1-h-long windows by using different frequency bands for the sensitivity analysis (see Results).

Statistical analysis of ambient noise (i.e., power spectral density–probability density functions or PSD–PDFs) and computation of a long-term spectrogram were performed according to the standard procedure of McNamara and Buland (2004). We used 6-min-long data segments, which overlap for 50% in each case. The data were instrument-corrected and differentiated into acceleration data. Computed PSDs were smoothed as 0.5-octave averages using 1/8 octave intervals and presented in dB (relative to $\mathrm{m}^2\,\mathrm{s}^{-4}\,\mathrm{Hz}^{-1}$). PDFs were generated for 0.5 dB bins using all the frequency spectra in the analyzed time interval.

We reconstructed a complete timeline of the 2019 OBS experiment using operators' notes, seismic, acoustic, and temperature records, and other direct evidence obtained in the field (E. van Dognen and R. Daorana, pers. comm., 2019).

RESULTS AND DISCUSSION

Timeline of Events

On August 5, the day of the planned OBS retrieval, the instrument did not release after the acoustic command was sent by a deck unit with a transceiver from the boat (Fig. 3a). The acoustic communication with the instrument showed that the command was properly received, and the release procedure was in progress. However, even ~8 h later, when operators returned to the site, the call to the instrument from the drop point showed that the instrument remained at the same depth. Eventually, the system was discovered floating in the fjord by a local hunter on August 7, and was 7 km from the drop point. The OBS was left on the coast and evacuated on August 9.

The timeline (Fig. 3a) shows that the OBS system descended in 183.5 s to the fjord seafloor (velocity = 1.32 m s^{-1}) on July 21 and ascended in 194 s (velocity = 1.25 m s^{-1}) on August 6. The anomalously long delay between the acoustic command and release was 9 h 39 min 28 s.

Bottom-Water Temperature

The mean bottom-water temperature in the fjord was -1.8 ± 0.1°C (Fig. 3b), which is, to our knowledge, among the coldest temperatures to date for an OBS deployment (Chen et al., 2019) and the coldest temperature to date for Bowdoin Fjord seafloor. This water corresponds to the Polar Water, i.e., relatively fresh and cold water of Arctic origin, brought by West Greenland Current which is sandwiched between the low-salinity, warm surface water and the warm, high-salinity water of Atlantic origin (Ohashi et al., 2020). This shows no evidence for incursion of warm Atlantic Water into the fjord, as observed in 2016 (Ohashi et al., 2020), which is an important driving mechanism for subaqueous glacier melting.

The temporal resolution and precision of the temperature data were limited. For example, it is difficult to estimate the possible impact of the July 29 calving event on water mixing and the possible corresponding temperature change. However, over the 15 days of the time-series, the water temperature was not constant. There was a statistically significant decrease (Fig. 3b) from $-1.6°C$ to $-1.9°C$ ($R^2 = 0.58$; F-statistic versus constant model: 3×10^4, p-value=0).

At the end of July 2019, one of the most significant surface melting and melt-water discharge episodes was observed in Greenland (Tedesco and Fettweis, 2020). Long-term mooring observations (at 1 km from the calving front; 181 m deep) showed anomalously cold water temperature in summer 2019 and were interpreted as downward shift of the cold layer due to thickening of a near-surface fresh water layer (Fujishi, 2020). Our record is consistent with this mechanism, although due to the limited duration of our observations, this evidence should be treated with caution. Nevertheless, since time-series of bottom-water temperatures in glacier fjords near calving fronts (<1 km) are extremely rare, this provides an impetus for future long-term OBS monitoring campaigns. Considering that seasonal variations of glacial terminuses (i.e., advance in winter due to less frontal ablation) are known from remote sensing, limited to ∼200 m in Northwest Greenland (Sakakibara and Sugiyama, 2020), and a glacier is not of a surging type, a risk of OBS scraping off the bottom by the advancing terminus can be avoided.

Seismic Activity

The complexity and diversity of seismic activity at the calving front is shown in Fig. 4. This example examines the beginning of a tremor-like calving signal, which apparently initiates with a precursory train of recurrent events having a high-frequency onset and low-frequency coda. In general, the seismic wavefield is almost continuously saturated by natural signals. Occasionally, we also observed high-frequency anthropogenic signals from boats and our instrumentation. For example, every 1.5 h, we detected a 23-s-long artificial tonal signal (∼57.5 Hz) with an up-sweeping onset and down-sweeping ending (Fig. 5). It was produced by the Hard Disk Drive (HDD) of the OBS, which stored data blocks every 1.5 h at ~3,450 rpm.

Natural events including impulsive high-frequency events, emergent low-frequency events, earthquake-like events with a high-frequency onset and low-frequency coda, monochromatic coda trains, and minutes-to-hours-long tremors are shown in Fig. 5. Their detailed analysis is beyond the scope of this paper; however, the observed intense seismic activity (Fig. 6) is lower compared with stations previously installed directly on ice, ~250 m from the calving front (Podolskiy et al., 2016). In particular, the overall number of seismic events detected with the STA/LTA algorithm (Fig. 6) is at least two times lower for the OBS (200 versus 400 events per hour) than for the on-ice stations (Podolskiy et al., 2016).

High- and low-pass-filtered time-series around an arbitrarily chosen frequency of 15 Hz revealed that, after July 31, a tide-modulated signal can be recognized especially well at higher frequencies (Fig. 6). The seismic signal is approximately in anti-phase with the tidal rates; i.e., when the tide is falling, the glacier accelerates (Sugiyama et al., 2015; van Dongen et al., 2021), which leads to increased seismicity due to extensional surface crevassing (Podolskiy et al., 2016, 2017). The tidal modulation is weaker, but similar to the one reported in Podolskiy et al. (2016). As might be expected, the OBS data are not completely independent of the near-surface glacier dynamics, but are less affected by it than the on-ice data. Here we acknowledge that the STA/LTA detections are sensitive to chosen parameters (for example, increasing the threshold for declaring the event up to 10 does not improve the tidal signal, but decreases the total number of events). Nevertheless, since our choice is consistent with the previous study by Podolskiy et al. (2016), the relative comparison is valid.

Noise Analysis

To quantify the frequency sensitivity of the seismometer, we used the unusual timeline of the experiment. In detail, we performed statistical analysis of noise for the following three stages: (A) at the fjord seafloor, (B) during free drift at the water surface; and (C) on the coast (Fig. 7). This analysis showed that our instrument can detect signals between ~0.05 Hz and the Nyquist frequency of 64 Hz. This frequency band corresponds to at least 10.32 octaves, which is relatively high considering the fundamental frequency of the seismometer is only 4.5 Hz.

Glacial Earthquake due to Iceberg Calving

On the morning of July 29, during a helicopter flight over the calving front, we observed that Bowdoin Fjord was covered with massive icebergs and ice mélange (Fig. 2c). Seismic data showed the highest amplitude seismic tremor between 03:42 UTC and 04:10 UTC (Fig. 8). Guided by our noise analysis and expectation that major capsizing calving events generate tens-second-long periods (e.g., Sergeant et al., 2019; Winberry et al., 2020), we bandpass-filtered the waveforms in different ranges from the lowest to highest possible frequency and computed a spectrogram.

The total duration of the unfiltered signal is ~25 min, which is mainly partitioned between three distinct phases (10, 2, and 5 min long; Phases 1, 2, and 3; Fig. 8). Each phase has characteristic features, indicating that different mechanisms generated each phase. In contrast to the calving event on July 25 (Fig. 4), this largest event had no distinguishable precursory seismicity immediately prior to calving. This implies that precursory seismic activity is not a ubiquitous characteristic of calving at Bowdoin Glacier.

Phases 1 and 3 have prominent long-period content (>2 s), which is lacking in Phase 2. Phase 2 is a monochromatic tremor with a characteristic high frequency of ~14 Hz (Fig. 8). The presence of energy at periods longer than 10 s suggests iceberg capsizing and is not typical of relatively small and rapid serac falls (Podolskiy and Walter, 2016). We suggest that the most complex Phase 1 corresponds to a rift propagation, separation of an iceberg, its consequent capsizing, and impact onto the ice cliff. Considering previously witnessed capsizing events at Bowdoin Glacier (July 8, 2017; https://www.youtube.com/watch?v=n6y4TKJJPeI), bottom-out rotation is likely, but can not be verified without numerical modeling. Phase 3 corresponds to disintegration of the main iceberg in the water, with further capsizing of its parts. Time-lapse photography is consistent with such an interpretation (Fig. B2): the 04:00 image shows the presence of a large iceberg overhead the OBS just before Phase 2, while the next image taken at 05:00 shows a disintegrated iceberg with no further changes in the calving front geometry.

The 2-min-long Phase 2 (Fig. 8) occurred before the major iceberg disintegration, during iceberg floatation over the OBS station. To our knowledge, there are no previous studies that report high-frequency monochromatic tremor during calving. MacAyeal et al. (2008) reported a seismic tremor with gliding spectral lines generated by two colliding tabular icebergs. However, the photograph taken approximately 2 mins after Phase 2 does not show a second major iceberg to suggest a similar interpretation (Fig. B2). Furthermore, no helicopter was in the area during this calving event. Prolonged avalanching of crushed ice into the water from the sloping iceberg is another possibility for Phase 2, or a turbidity current induced by full-depth iceberg overturn and sediment passing over the OBS. Debris precipitation from the iceberg is a less likely interpretation, because any small stones hitting the OBS should produce sudden events of variable amplitude. However, it is unclear if fine, sand-like precipitation can produce the 14 Hz tremor (e.g., fine sediments were discovered within the OBS at retrieval, as detailed below).

For large calving events, their long periods are known to propagate as surface waves over teleseismic distances (Podolskiy and Walter, 2016; Sergeant et al., 2019; Winberry et al., 2020). The closest permanent seismic stations (TULEG and NEEM; DK/GLISN network) are located 125 km to the south and 419 km to the east of Bowdoin Glacier (Fig. 9a). The highest long-period amplitude was observed by the OBS during Phase 1 at 03:49:18 UTC. Assuming a Rayleigh wave velocity with a 20 s period is $3.5\,\mathrm{km\,s^{-1}}$ (Mordret, 2018), we can expect a 36-s-delayed arrival to TULEG. At 03:50:00, TULEG detected a dispersed low-frequency signal (Fig. 9b). Some energy was also present at higher frequencies between 1 and 15 Hz (Fig. B3). Phases 2 and 3 are not clearly recognizable at TULEG, as might be expected for iceberg processes in water, and without direct coupling to the crust. The low-frequency signal could be detected as far as NEEM station (Fig. 9c). We were not able to recognize this glacial earthquake at distances of >450 km (e.g., at the GLISN stations KULLO, EUNU, and ALE).

This long-period seismic signal is typical for major non-tabular calving events in Greenland, and indicates that the terminus is in a near-grounded state (i.e., floating ice tongues do not generate glacial earthquakes; (Sergeant et al., 2019)) which is consistent with our current understanding of the calving front.

Delayed Release and Sediments

During disassembly of the OBS, a large amount of soft sediment (i.e., glacial till) was found within the instrument's protective shell (Fig. 10). This was unexpected considering that the slits and holes in the shell were taped closed and seemingly too small to allow injection of this amount of sediment. A similar observation was reported for an experiment of nearly the same duration using a bottom lander at an oceanographic mooring near the calving front of LeConte Glacier, southeast Alaska (Nash et al., 2020). The lander had a 3-cm-thick layer of glacial sediments on it. In this regard, several points are important to report:

1. In general, extremely high sedimentation rates have been found in glacier fjords (Howe et al., 2010; Boldt et al., 2013). Rates of glacial sediment accumulation are lower at high latitudes, but in temperate climates can be meters per year close to the glacier termini (Boldt et al., 2013). At Bowdoin Fjord, turbid subglacial discharge plumes are known to bring sediments to the surface and then deposit them downstream (Kanna et al., 2018). High sedimentation rates are also a cause of sediment softness when a thick, muddy layer with a high water content is present.
2. It is possible that the full-depth calving event on July 29 induced a turbidity current and submarine sediment avalanches. There is direct evidence for potentially strong water mixing in the fjord, because a pulse of high current corresponding to the timing of calving was recorded 1 km away

from the calving front by a long-term oceanographic mooring at 181 m depth (Fujishi, 2020).

3. The fact that the calved iceberg passed over the OBS and disintegrated suggests possible intense precipitation of a glacier till from the debris-laden sole of the iceberg.

These points suggest that soft sediments could have been the main reason for the OBS release delay. The likely effect of the sediment is the insulation of the release necks from contact with seawater. The process of current-induced corrosion is needed to cut the necks from the anchor (followed by separation of the buoyant OBS system), which usually takes 10–15 min. To our knowledge, it does not depend on the water temperature, but requires ions (i.e., salt) to allow the current, and thus this process does not work in fresh water. Purely fresh water is primarily supplied by subglacial discharge plumes near the calving front. However, due to buoyancy-driven convection, such water is quickly mixed with saline ambient water and upwelled along the ice cliff to the surface. This implies that due to a strong positive buoyancy, fresh water cannot remain at the bottom of the fjord. From the previous oceanographic profiling in the Bowdoin Fjord and mooring observations in July 2019, it is known that at the depth of OBS deployment the salinity was at least 33.5 PSU (Ohashi et al., 2020; Fujishi, 2020). Therefore, we suggest that the low salinity is an unlikely candidate for the delayed release.

When the necks are submerged and covered by sediment, the contact with seawater is dramatically reduced proportionally to the density of the sediment. The necks are only 120 mm above the landing plane of the instrument. Their complete submergence into soft sediment is possible at landing and/or due to additional sedimentation over the following two weeks. The observed delay of $\sim$9 h 39 min was $\sim$46 times longer than usual, and has never been experienced during our previous OBS deployments in the Pacific and Atlantic oceans.

A straightforward strategy for dealing with the deep-sediment issue is to use OBS systems with conceptually different release mechanisms. For example, modern OBS systems such as NAMMU by KUM (Germany). However, for updating an already existing instrument pool like ours this is not feasible, because OBS are expensive instruments. Alternatively, one could rely on the following strategies:

1. Include a satellite Iridium/GPS tracking system for search and rescue of re-surfaced OBSs as used, for example, by Aquarius.
2. Use an underwater ROV for inspection and identification of problems. For example, for shallow-water (i.e., 100–300 m), there are commercially available and relatively affordable high-performance ROVs like BlueROV2 by BlueRobotics or SRV-8 by Oceanbotics (both from the USA).
3. Finally, particularly soft mud is expected over the areas of recent glacier retreat. Therefore, by increasing the distance to the calving front, the sediment effect should be reduced. However, this option would result in attenuation of seismic waves with increasing distance from the glacier and should be considered on a case-by-case basis. Indeed, sub-bottom profiling would be invaluable to find an appropriate deployment site and avoid locations of soft sediments. However, it is difficult to conduct near the calving fronts due to ice conditions and calving.

CONCLUDING REMARKS

We have described an OBS experiment in front of a tidewater calving glacier in Greenland. This multi-purpose deployment yielded unique time-series of temperature, seismicity, and underwater sound in a challenging oceanographic zone. Our main conclusions are:

- We demonstrated the feasibility of deploying an OBS near the calving front of a tide-water glacier and showed the low levels of high-frequency noise underwater (Fig. 7). This highlights that this approach has practical potential for investigating basal processes.

- We found a gradual decrease in water temperature, presumably due to modification of fjord water stratification caused by extreme surface melting.

- We obtained the first near-source underwater seismic record of calving that generated a glacial earthquake detectable 419 km away; this revealed a complex iceberg detachment and disintegration history, including a previously unreported monochromatic tremor at ∼14 Hz. This shows the difficulty in using regional seismic networks to grasp the calving process fully and provides an impetus for considering tremors as indicators of iceberg activity overhead and, possibly, as a gauge for sedimentation rates.

- Soft glacial sediment on the near-terminus fjord seafloor can affect instrument deployment and retrieval.

Regarding the latter point, we note that the key issue with non-return of complex and expensive oceanographic instrumentation is our inability to identify the reason for failure *a posteriori*. Therefore, our experiences and approach should be useful for geoscientists working at glacial margins, and ultimately lead to a new methodology of monitoring glacial calving and basal seismicity. Finally, the study contributes to ongoing multi-disciplinary efforts to understand rapidly changing ice, ocean, and coastal environments of the northwestern Greenland (Sugiyama et al., 2020).

DATA AND RESOURCES

OBS data are publicly available through the Arctic Data archive System website (https://ads.nipr.ac.jp/dataset/; A20200108-002). TULEG and NEEM data were downloaded through the IRIS Web Services (https://www.iris.edu/hq/programs/glisn). Pituffik sea-level data were retrieved from the Global Sea Level Observing System network (http://www.ioc-sealevelmonitoring.org/) The time-lapse imagery is directly presented in the figures. The analysis was conducted, and the plots were produced, using the “win2sac” program (http://wwweic.eri.u-tokyo.ac.jp/WIN/pub/win/), Matlab R2018b (https://mathworks.com/products/matlab.html) and the Matplotlib and ObsPy Python libraries (Hunter, 2007; Krischer et al., 2015).

ACKNOWLEDGEMENTS

We thank E. van Dongen for providing time-lapse images, as well as discussions on calving, and T. Ando for discussions and photographs of sediment coring. We thank Air Greenland helicopter pilots and F. Walter, G. Jouvet, F. Lindner, A. Bauder, and J. Wassermann for logistical and technical support in 2019. We also thank colleagues (I. Asaji, T. Ando, Y. Sakuragi, A. Mangeney, and O. Castelnau) and local guides (T. Oshima, K. Petersen, Q. Aladaq, S. Aladaq, and R. Daorana) for their assistance during fieldwork. Finally, we thank the two anonymous reviewers, and the editors, M. Pirli and A. Bent, for helping us to improve the manuscript. The Ministry for Nature, Environment, and Justice (Government of Greenland) granted permission (C-19-37) to conduct this fieldwork. This work and N.K. were supported by an Arctic Challenge for Sustainability (ArCS) research project (JPMXD1300000000) and ArCS-II (JPMXD1420318865) research project funded by the Ministry of Education, Culture, Sports, Science, and Technology of Japan (MEXT), J-ARC Net, Grants-in-Aid for Scientific Research “KAKENHI” (18K18175), and the Second Earthquake and Volcano Hazards Observation and Research Program (Earthquake and Volcano Hazard Reduction Research funded by MEXT).

REFERENCES

Au, W.W.L., Lammers, M.O.E., 2016. Listening in the Ocean. Modern Acoustics and Signal Processing, Springer-Verlag. doi:10.1007/978-1-4939-3176-7.

Azuma, R., Murai, Y., Katsumata, K., Nishimura, Y., Yamada, T., Mochizuki, K., Shinohara, M., 2012. Was the 1952 tokachi-oki earthquake (mw= 8.1) a typical underthrust earthquake?: Plate interface reflectivity measurement by an air gun–ocean bottom seismometer experiment in the kuril trench. Geochemistry, Geophysics, Geosystems 13.

Bamber, J.L., Oppenheimer, M., Kopp, R.E., Aspinall, W.P., Cooke, R.M., 2019. Ice sheet contributions to future sea-level rise from structured expert judgment. Proceedings of the National Academy of Sciences 116, 11195–11200. doi:10.1073/pnas.1817205116.

Beroza, G.C., Ide, S., 2011. Slow earthquakes and nonvolcanic tremor. Annual review of Earth and planetary sciences 39, 271–296.

Bjørk, A.A., Kruse, L.M., Michaelsen, P.B., 2015. Getting Greenland's glaciers right – a new data set of all official Greenlandic glacier names. The Cryosphere 9, 2215–2218.

Boldt, K.V., Nittrouer, C.A., Hallet, B., Koppes, M.N., Forrest, B.K., Wellner, J.S., Anderson, J.B., 2013. Modern rates of glacial sediment accumulation along a 15° S-N transect in fjords from the Antarctic Peninsula to southern Chile. Journal of Geophysical Research: Earth Surface 118, 2072–2088. doi:https://doi.org/10.1002/jgrf.20145.

Chen, Z., Bromirski, P.D., Gerstoft, P., Stephen, R.A., Lee, W.S., Yun, S., Olinger, S.D., Aster, R.C., Wiens, D.A., Nyblade, A.A., 2019. Ross ice shelf icequakes associated with ocean gravity wave activity. Geophysical Research Letters 46, 8893–8902. doi:https://doi.org/10.1029/2019GL084123.

Clinton, J.F., Nettles, M., Walter, F., Anderson, K., Dahl-Jensen, T., Giardini, D., Govoni, A., Hanka, W., Lasocki, S., Lee, W.S., McCormack, D., Mykkelveit, S., Stutzmann, E., Tsuboi, S., 2014. Real-time geophysical data enhance earth system monitoring in greenland. Eos Trans. 95, 13–14.

Deane, G., Glowacki, O., Stoles, M., Pettit, E., 2019. The underwater sounds of glaciers. Acoustics Today 15, 12–19. doi:10.1121/AT.2019.15.4.12.

van Dongen, E.C.H., Jouvet, G., Sugiyama, S., Podolskiy, E.A., Funk, M., Benn, D.I., Lindner, F., Bauder, A., Seguinot, J., Leinss, S., Walter, F., 2021. Thinning leads to calving-style changes at bowdoin glacier, greenland. The Cryosphere , 1–28doi:10.5194/tc-2020-252.

Dreo, R., Bouffaut, L., Leroy, E., Barruol, G., Samaran, F., 2019. Baleen whale distribution and seasonal occurrence revealed by an ocean bottom seismometer network in the western indian ocean. Deep Sea Research Part II: Topical Studies in Oceanography 161, 132–144. doi:10.1016/j.dsr2.2018.04.005.

Dziak, R.P., Lee, W.S., Haxel, J.H., Matsumoto, H., Tepp, G., Lau, T.K., Roche, L., Yun, S., Lee, C.K., Lee, J., Yoon, S.T., 2019. Hydroacoustic, meteorologic and seismic observations of the 2016 nansen ice shelf calving event and iceberg formation. Frontiers in Earth Science 7, 183. doi:10.3389/feart.2019.00183.

Frankinet, B., Lecocq, T., Camelbeeck, T., 2020. Wind-induced seismic noise at the Princess Elisabeth Antarctica Station. The Cryosphere Discussions 2020, 1–16. doi:10.5194/tc-2020-267.

Frouin-Mouy, H., Kowarski, K., Martin, B., Bröker, K., 2017. Seasonal Trends in Acoustic Detection of Marine Mammals in Baffin Bay and Melville Bay, Northwest Greenland. Arctic 70, 59–76. doi:10.14430/arctic4632.

Fujishi, Y., 2020. Seasonal variability of ocean temperature, salinity and current in Bowdoin Fjord in northwest Greenland. Master's thesis. Hokkaido University. Sapporo, Japan.

Hable, S., Sigloch, K., Barruol, G., Stähler, S.C., Hadziioannou, C., 2018. Clock errors in land and ocean bottom seismograms: high-accuracy estimates from multiple-component noise cross-correlations. Geophysical Journal International 214, 2014–2034. doi:10.1093/gji/ggy236.

Howe, B.M., Miksis-Olds, J., Rehm, E., Sagen, H., Worcester, P.F., Haralabus, G., 2019. Observing the oceans acoustically. Frontiers in Marine Science 6, 426. doi:10.3389/fmars.2019.00426.

Howe, J.A., Austin, W.E.N., Forwick, M., Paetzel, M., Harland, R., Cage, A.G., 2010. Fjord systems and archives: a review. Geol. Soc. London, Spec. Publ. 344, 5–15. doi:10.1144/SP344.2.

Hudson, T.S., Brisbourne, A.M., Walter, F., Gräff, D., White, R.S., Smith, A.M., 2020. Icequake source mechanisms for studying glacial sliding. Journal of Geophysical Research: Earth Surface 125, e2020JF005627. doi:https://doi.org/10.1029/2020JF005627.

Hunter, J.D., 2007. Matplotlib: A 2d graphics environment. Comput. Sci. Eng. 9, 90–95. doi:10.1109/MCSE.2007.55.

Kanna, N., Sugiyama, S., Ohashi, Y., Sakakibara, D., Fukamachi, Y., Nomura, D., 2018. Upwelling of macronutrients and dissolved inorganic carbon by a subglacial freshwater driven plume in Bowdoin Fjord, Northwestern Greenland. J. Geophys. Res. Biogeo. 123, 1666–1682. doi:10.1029/2017JG004248.

Krischer, L., Megies, T., Barsch, R., Beyreuther, M., Lecocq, T., Caudron, C., Wassermann, J., 2015. ObsPy: a bridge for seismology into the scientific Python ecosystem. Comput. Sci. Discov. 8, n/a–n/a. doi:10.1088/1749-4699/8/1/014003. 014003.

Lipovsky, B.P., Dunham, E.M., 2017. Slow-slip events on the whillans ice plain, antarctica, described using rate-and-state friction as an ice stream sliding law. Journal of Geophysical Research: Earth Surface 122, 973–1003.

Lydersen, C., Assmy, P., Falk-Petersen, S., Kohler, J., Kovacs, K.M., Reigstad, M., Steen, H., Strøm, H., Sundfjord, A., Varpe, Ø., Walczowski, W., Weslawski, J.M., Zajaczkowski, M., 2014. The importance of tidewater glaciers for marine mammals and seabirds in Svalbard, Norway. J. Marine Syst. 129, 452–471. doi:https://doi.org/10.1016/j.jmarsys.2013.09.006.

MacAyeal, D.R., Okal, E.A., Aster, R.C., Bassis, J.N., 2008. Seismic and hydroacoustic tremor generated by colliding icebergs. Journal of Geophysical Research 113, F03011. doi:10.1029/2008JF001005.

Machida, Y., Shinohara, M., Takanami, T., Murai, Y., Yamada, T., Hirata, N., Suyehiro, K., Kanazawa, T., Kaneda, Y., Mikada, H., Sakai, S., Watanabe, T., Uehira, K., Takahashi, N., Nishino, M., Mochizuki, K., Sato, T., Araki, E., Hino, R., Uhira, K., Shiobara, H., Shimizu, H., 2009. Heterogeneous structure around the rupture area of the 2003 tokachi-oki earthquake (mw=8.0), japan, as revealed by aftershock observations using ocean bottom seismometers. Tectonophysics 465, 164 – 176.

McNamara, D.E., Buland, R.P., 2004. Ambient Noise Levels in the Continental United States. BSSA 94, 1517–1527.

Minowa, M., Podolskiy, E.A., Jouvet, G., Weidmann, Y., Sakakibara, D., Tsutaki, S., Genco, R., Sugiyama, S., 2019. Calving flux estimation from tsunami waves. Earth Planet. Sci. Lett. 515, 283–290. doi:10.1016/j.epsl.2019.03.023.

Mordret, A., 2018. Uncovering the iceland hot spot track beneath greenland. Journal of Geophysical Research: Solid Earth 123, 4922–4941. doi:https://doi.org/10.1029/2017JB015104.

Munk, W., Worcester, P., Wunsch, C., 1995. Ocean Acoustic Tomography. Cambridge Monographs on Mechanics, Cambridge University Press. doi:10.1017/CBO9780511666926.

Nash, J., Pettit, E., Spain, P., 2020. Adcps aid pioneering study of how glaciers melt. Environment Coastal & Offshore - ECO Polar n/a, 104–107.

Obara, K., 2002. Nonvolcanic deep tremor associated with subduction in southwest japan. Science 296, 1679–1681.

Ohashi, Y., Aoki, S., Matsumura, Y., Sugiyama, S., Kanna, N., Sakakibara, D., 2020. Vertical distribution of water mass properties under the influence of subglacial discharge in Bowdoin Fjord, northwestern Greenland. Ocean Sci. 16, 545–564. doi:10.5194/os-16-545-2020.

Pettit, E.C., Lee, K.M., Brann, J.P., Nystuen, J.A., Wilson, P.S., O'Neel, S., 2015. Unusually loud ambient noise in tidewater glacier fjords: A signal of ice melt. Geophysical Research Letters 42, 2309–2316. doi:10.1002/2014GL062950.

Podolskiy, E.A., 2020. Toward the acoustic detection of two-phase flow patterns and helmholtz resonators in englacial drainage systems. Geophysical Research Letters 47, e2020GL086951.

Podolskiy, E.A., Genco, R., Sugiyama, S., Walter, F., Funk, M., Minowa, M., Tsutaki, S., Ripepe, M., 2017. Seismic and infrasonic monitoring of Bowdoin Glacier, Greenland. Low Temperature Science 75, 15–36.

Podolskiy, E.A., Sugiyama, S., 2020. Soundscape of a Narwhal Summering Ground in a Glacier Fjord (Inglefield Bredning, Greenland). Journal of Geophysical Research: Oceans 125, e2020JC016116.

Podolskiy, E.A., Sugiyama, S., Funk, M., Walter, F., Genco, R., Tsutaki, S., Minowa, M., Ripepe, M., 2016. Tide-modulated ice flow variations drive seismicity near the calving front of Bowdoin Glacier, Greenland. Geophys. Res. Lett. 43, 2036–2044. doi:10.1002/2016GL067743. 2016GL067743.

Podolskiy, E.A., Walter, F., 2016. Cryoseismology. Rev. Geophys. 54, 708–758. 2016RG000526.

Riera, A., Rountree, R.A., Pine, M.K., Juanes, F., 2018. Sounds of Arctic cod (Boreogadus saida) in captivity: A preliminary description. The Journal of the Acoustical Society of America 143, EL317–EL321. doi:10.1121/1.5035162.

Rouet-Leduc, B., Hulbert, C., Johnson, P., 2019. Continuous chatter of the Cascadia subduction zone revealed by machine learning. Nature Geosci. 12, 75–79.

Russel, J., Eilo, Z., Mosher, S., 2019. OBSrange: A new tool for the precise remote location of Ocean-Bottom Seismometers. Seismological Research Letters 90, 1627–1641. doi:10.1785/0220180336.

Sakakibara, D., Sugiyama, S., 2020. Seasonal ice-speed variations in 10 marine-terminating outlet glaciers along the coast of prudhoe land, northwestern greenland. Journal of Glaciology 66, 25–34. doi:10.1017/jog.2019.81.

Schulz, M., Berger, W.H., Jansen, E., 2008. Listening to glaciers. Nature Geoscience 1, 408–408. doi:10.1038/ngeo235.

Sergeant, A., Mangeney, A., Yastrebov, V.A., Walter, F., Montagner, J.P., Castelnau, O., Stutzmann, E., Bonnet, P., Ralaiarisoa, V.J.L., Bevan, S., et al., 2019. Monitoring greenland ice sheet buoyancy-driven calving discharge using glacial earthquakes. Annals of Glaciology 60, 75–95. doi:10.1017/aog.2019.7.

Shinohara, M., Kanazawa, T., Yamada, T., Nakahigashi, K., Sakai, S., Hino, R., Murai, Y., Yamazaki, A., Obana, K., Ito, Y., Iwakiri, K., Miura, R., Machida, Y., Mochizuki, K., Uehira, K., Tahara, M., Kuwano, A., Amamiya, S., Kodaira, S., Takanami, T., Kaneda, Y., Iwasaki, T., 2008. Precise aftershock distribution of the 2007 chuetsu-oki earthquake obtained by using an ocean bottom seismometer network. Earth, Planets and Space 60, 1121–1126.

Shinohara, M., Yamada, T., Nakahigashi, K., Sakai, S., Mochizuki, K., Uehira, K., Ito, Y., Azuma, R., Kaiho, Y., No, T., Shiobara, H., Hino, R., Murai, Y., Yakiwara, H., Sato, T., Machida, Y., Shinbo, T., Isse, T., Miyamachi, H., Obana, K., Takahashi, N., Kodaira, S., Kaneda, Y., Hirata, K., Yoshikawa, S., Obara, K., Iwasaki, T., Hirata, N., 2011. Aftershock observation of the 2011 off the pacific coast of tohoku earthquake by using ocean bottom seismometer network. Earth, Planets and Space 63, 59.

Straneo, F., Sutherland, D.A., Stearns, L., Catania, G., Heimbach, P., Moon, T., Cape, M.R., Laidre, K.L., Barber, D., Rysgaard, S., Mottram, R., Olsen, S., Hopwood, M.J., Meire, L., 2019. The case for a sustained greenland ice sheet-ocean observing system (grioos). Frontiers in Marine Science 6, 138. doi:10.3389/fmars.2019.00138.

Sugiyama, S., Kanna, N., Sakakibara, D., Ando, T., Asaji, I., Kondo, K., Wang, Y., Fujishi, Y., Fukumoto, S., Podolskiy, E., Fukamachi, Y., Takahashi, M., Matoba, S., Iizuka, Y., Greve, R., Furuya, M., Tateyama, K., Watanabe, T., Yamasaki, S., Yamaguchi, A., Nishizawa, B., Matsuno, K., Nomura, D., Sakuragi, Y., Matsumura, Y., Ohashi, Y., Aoki, T., Niwano, M., Hayashi, N., Minowa, M., Jouvet, G., van Dongen, E., Bauder, A., Funk, M., Bjørk, A.A., Oshima, T., 2020. Rapidly changing glaciers, ocean and coastal environments, and their impact on human society in the Qaanaaq region, northwestern Greenland. Polar Science , 100632doi:https://doi.org/10.1016/j.polar.2020.100632.

Sugiyama, S., Sakakibara, D., Tsutaki, S., Maruyama, M., Sawagaki, T., 2015. Glacier dynamics near the calving front of Bowdoin Glacier, northwestern Greenland. J. Glaciol. 61, 223–232.

Tedesco, M., Fettweis, X., 2020. Unprecedented atmospheric conditions (1948–2019) drive the 2019 exceptional melting season over the Greenland ice sheet. The Cryosphere 14, 1209–1223. doi:10.5194/tc-14-1209-2020.

Todd, E.K., Schwartz, S.Y., Mochizuki, K., Wallace, L.M., Sheehan, A.F., Webb, S.C., Williams, C.A., Nakai, J., Yarce, J., Fry, B., Henrys, S., Ito, Y., 2018. Earthquakes and tremor linked to seamount subduction during shallow slow slip at the hikurangi margin, new zealand. Journal of Geophysical Research: Solid Earth 123, 6769–6783. doi:https://doi.org/10.1029/2018JB016136.

Webb, S.C., 1998. Broadband seismology and noise under the ocean. Reviews of Geophysics 36, 105–142.

Winberry, J.P., Huerta, A.D., Anandakrishnan, S., Aster, R.C., Nyblade, A.A., Wiens, D.A., 2020. Glacial earthquakes and precursory seismicity associated with thwaites glacier calving. Geophysical Research Letters 47, e2019GL086178. doi:https://doi.org/10.1029/2019GL086178.

Worcester, P., Dzieciuch, M., Sagen, H., 2020. Ocean acoustics in the rapidly changing arctic. Acoustics Today 16, 55–64. doi:10.1121/AT.2020.16.1.55.

Zoet, L.K., Ikari, M.J., Alley, R.B., Marone, C., Anandakrishnan, S., Carpenter, B.M., Scuderi, M.M., 2020. Application of constitutive friction laws to glacier seismicity. Geophysical Research Letters 47, e2020GL088964. doi:https://doi.org/10.1029/2020GL088964.

Zoet, L.K., Iverson, N.R., 2020. A slip law for glaciers on deformable beds. Science 368, 76–78.

Evgeny A. Podolskiy
Arctic Research Center / GiCORE
Hokkaido University
Kita-21 Nishi-11, Kita-ku
Sapporo, Hokkaido 001-0021, Japan
evgeniy.podolskiy@gmail.com

Yoshio Murai
Institute of Seismology and Volcanology, Faculty of Science
Hokkaido University
Kita-10 Nishi-8, Kita-ku
Sapporo, Hokkaido 060-0810, Japan

Naoya Kanna
Atmosphere and Ocean Research Institute
University of Tokyo
5-1-5, Kashiwanoha
Kashiwa, Chiba 277-8564, Japan

Shin Sugiyama
Institute of Low Temperature Science
Hokkaido University
Kita-19, Nishi-8, Kita-ku
Sapporo, Hokkaido 060-0819, Japan

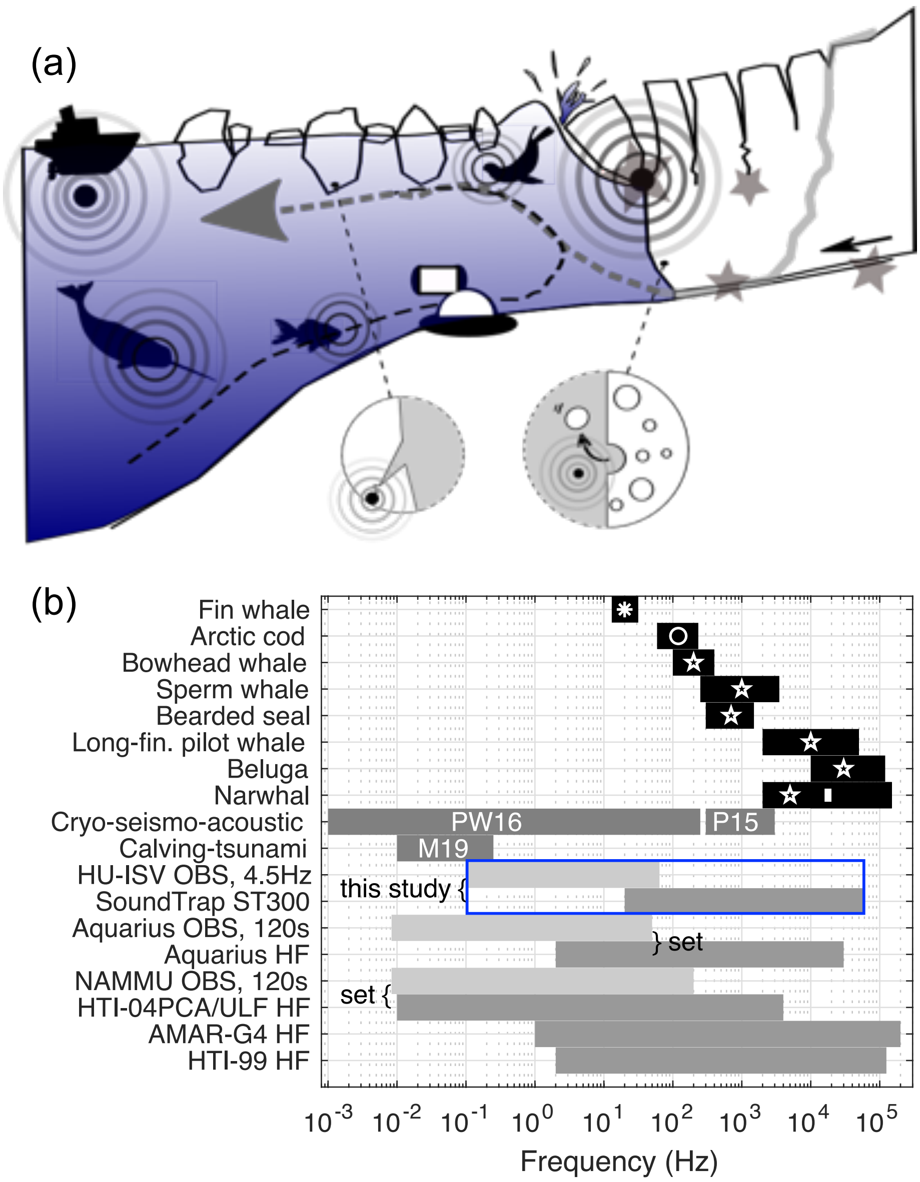

Figure 1: **(a)** Schematic of the main seismo-acoustic sources in a glacier fjord, which can be studied using an ocean-bottom seismometer (OBS) equipped with a hydrophone. Stars indicate the main seismic sources (iceberg calving, crevassing, sliding, and melt-water tremor; (Podolskiy and Walter, 2016)); circles correspond to the main acoustic sources (animals, anthropogenic noise, bubble melt-out, and ice cracking; (Pettit et al., 2015; Frouin-Mouy et al., 2017; Riera et al., 2018)). The arrow shows the principal water circulation. **(b)** Characteristic frequencies of sounds by both marine mammal/fish species in Greenlandic waters, and the seismo-acoustic processes related to ice and iceberg-generated tsunamis, as well as the frequency bandwidths of the state-of-the-art seismo-acoustic instruments used here ("this study") and available internationally ("set" implies a coupled system). Labels and symbols indicate the corresponding references: $*$ = Dreo et al. (2019), $\circ$ = Riera et al. (2018), "P15" = Pettit et al. (2015), "M19" = Minowa et al. (2019), "PW16" = Podolskiy and Walter (2016), and $\star$ = Frouin-Mouy et al. (2017) (the white bar marks the frequency that helps to distinguish narwhal calls from its closest relative [i.e., the beluga whale]).

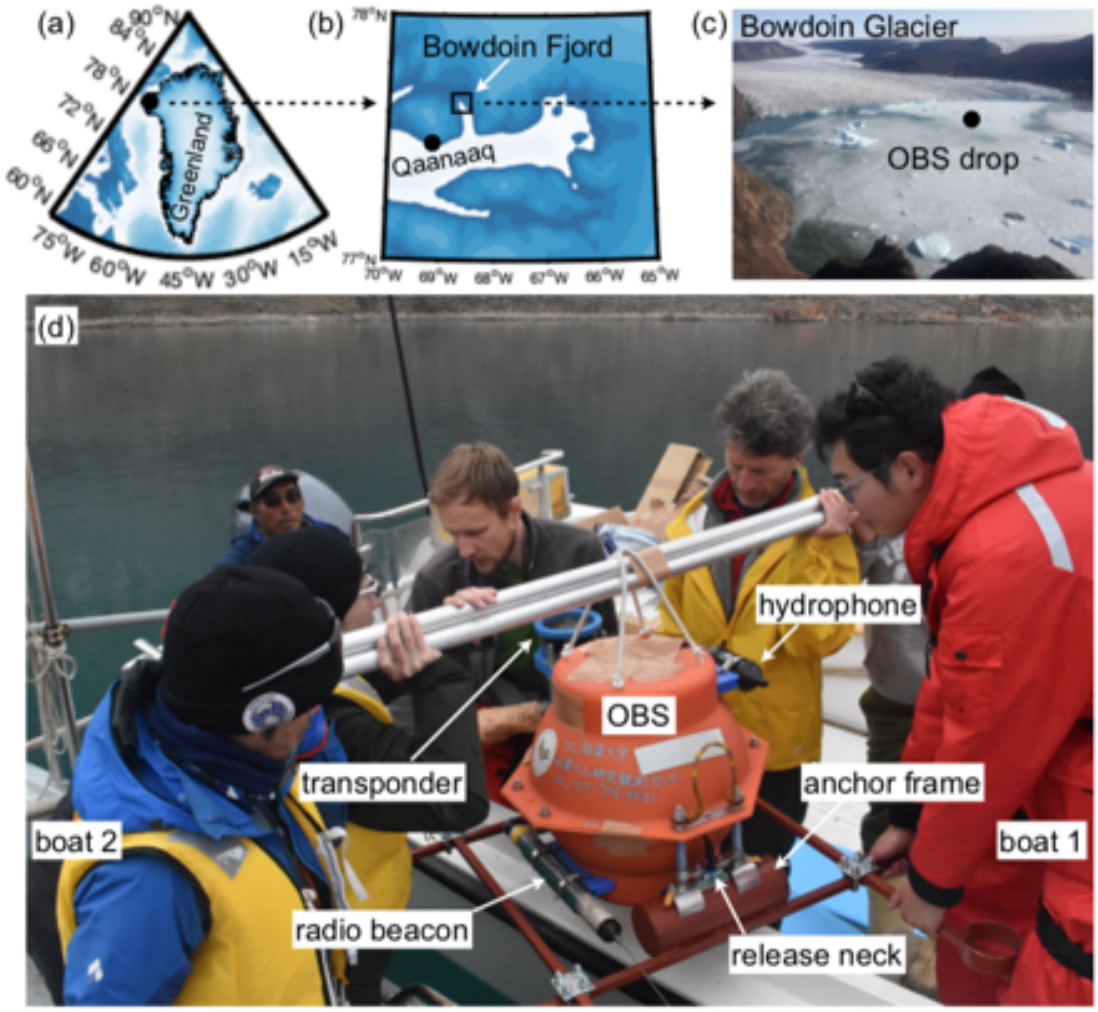

Figure 2: **(a)** Location of the study site in Greenland. **(b)** Inglefield Bredning and Bowdoin fjords. **(c)** Calving front of Bowdoin Glacier with the OBS drop point (credit: E. A. Podolskiy; July, 29, 2019). **(d)** Rehearsal of the OBS placement between parallel-parked boats in Falcon Bay, Bowdoin Fjord, for manual OBS deployment in front of the calving front (credit: I. Asaji; July 21, 2019).

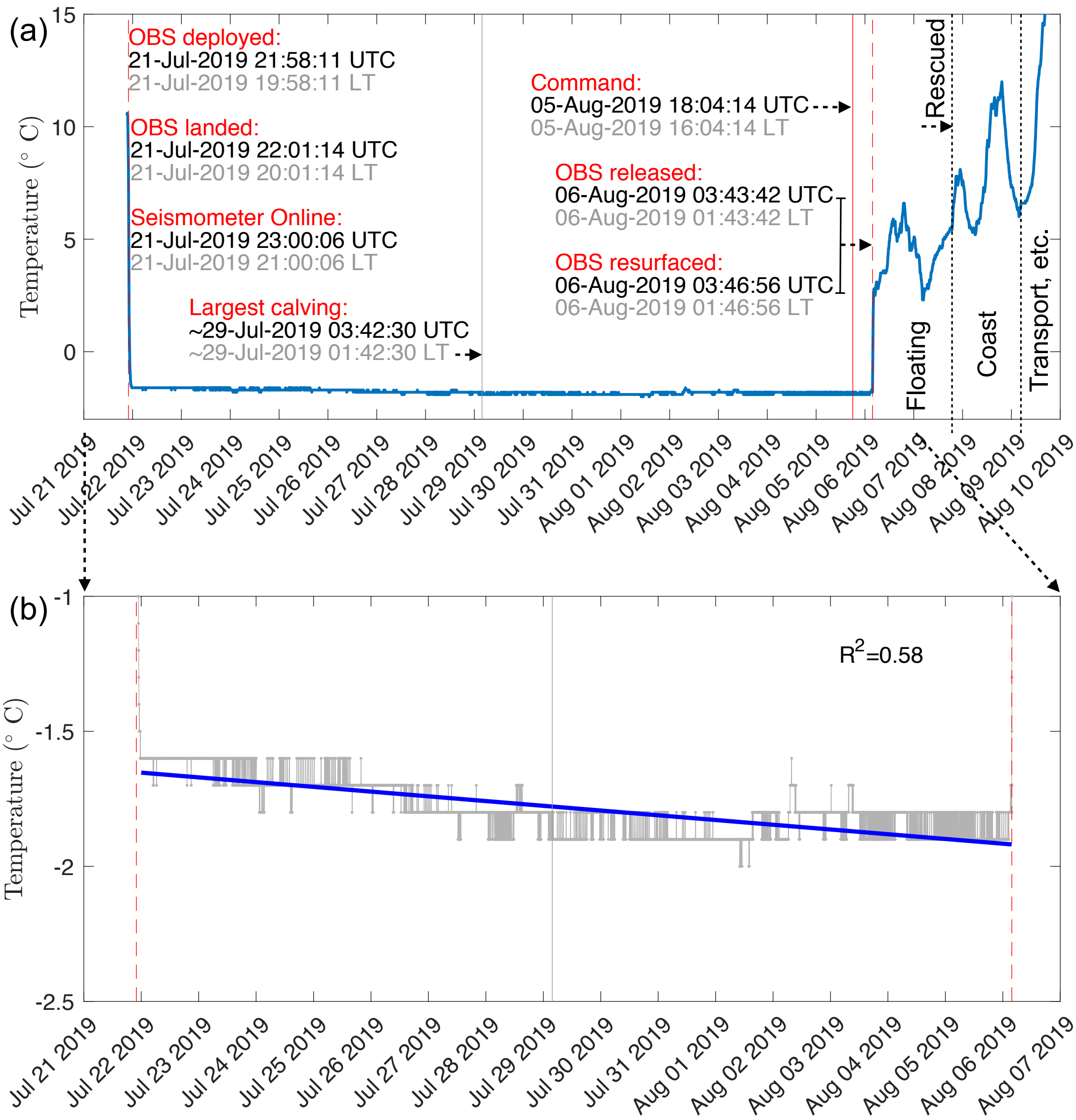

Figure 3: **(a)** Timeline of the 2019 OBS experiment in Bowdoin Fjord marked on a time-series of temperature (recorded by the SoundTrap's thermistor) in UTC time. **(b)** Enlarged view of the temperature for a period of recording at the seafloor in Bowdoin Fjord. A linear regression model (ordinary least-squares fit) is shown in blue (for undisturbed observations between July 22, 00:00, and the time of release; n = 21,823).

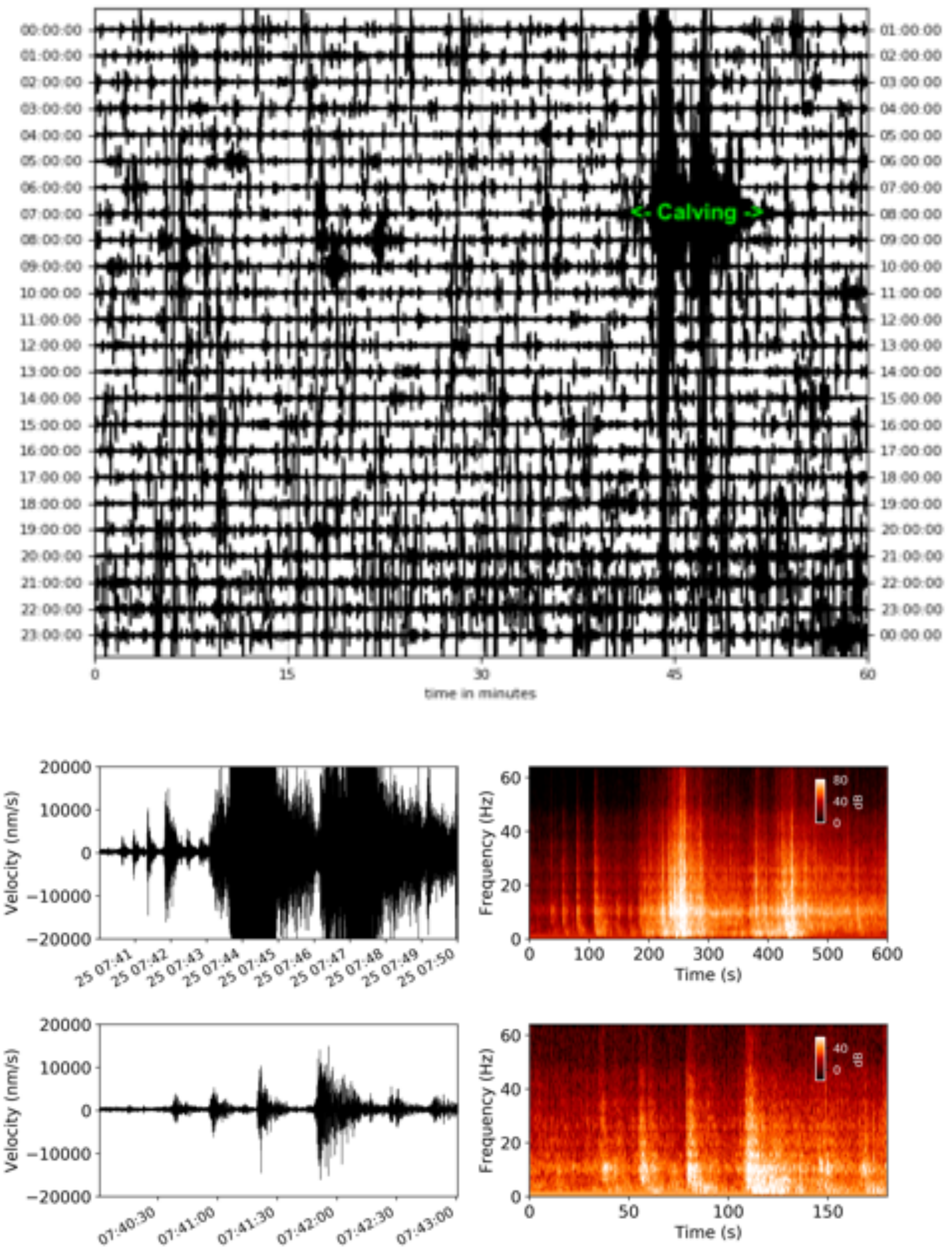

Figure 4: Day-long example of intense and diverse seismic activity revealed by the raw OBS data (vertical component; July 25, 2019; UTC). The highest amplitude ∼7-min-long event from 07:43 is an iceberg calving event at the northwestern side of the terminus (this event and its initiation are enlarged in the lower subpanels).

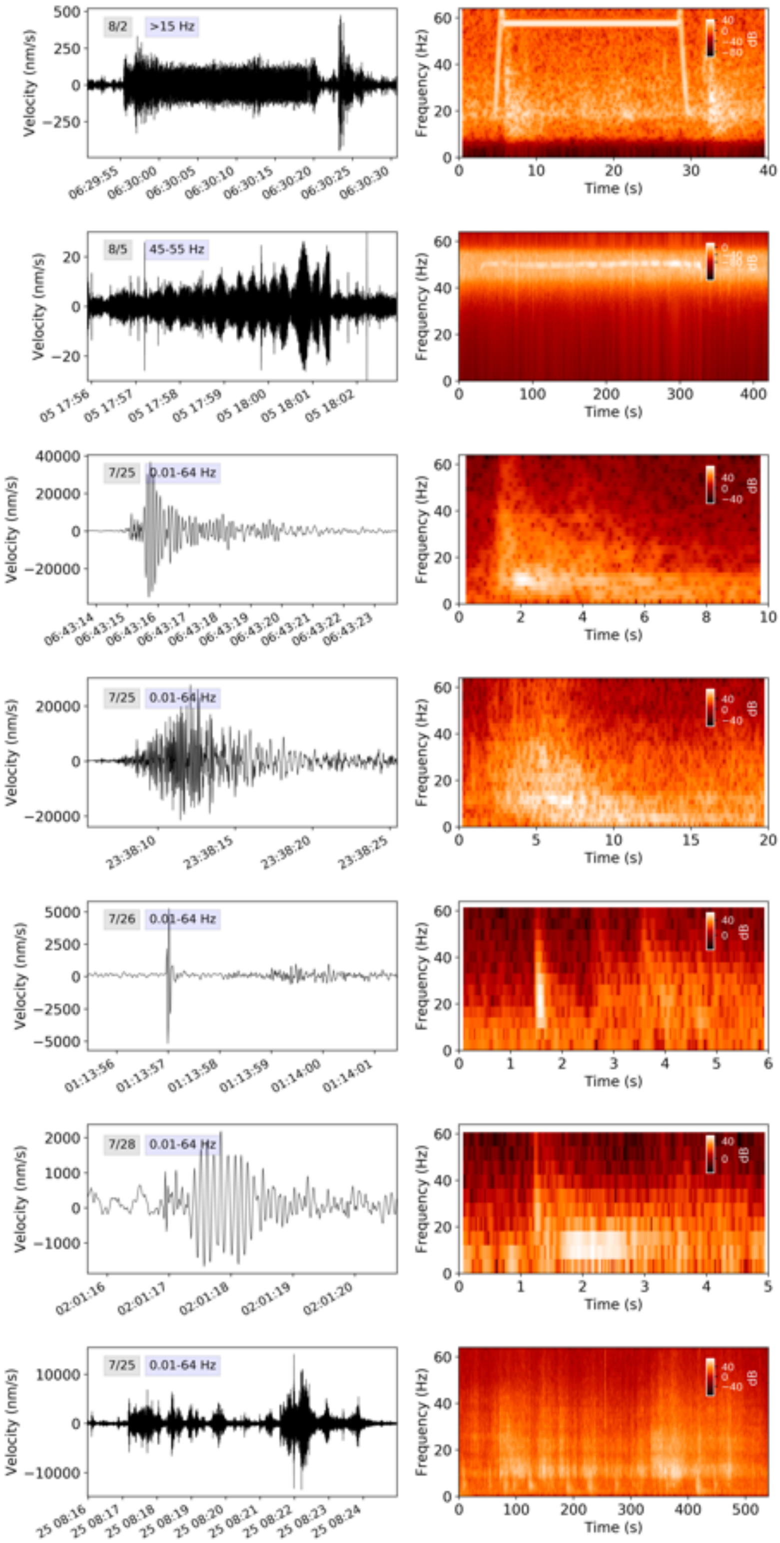

Figure 5: Diversity of OBS-recorded events (waveforms and their spectrograms). The upper left corner of each waveform subplot indicates the date (MM/DD) and the frequency band shown. The upper two subpanels show the HDD ping and boat tremor, respectively; the rest are natural events.

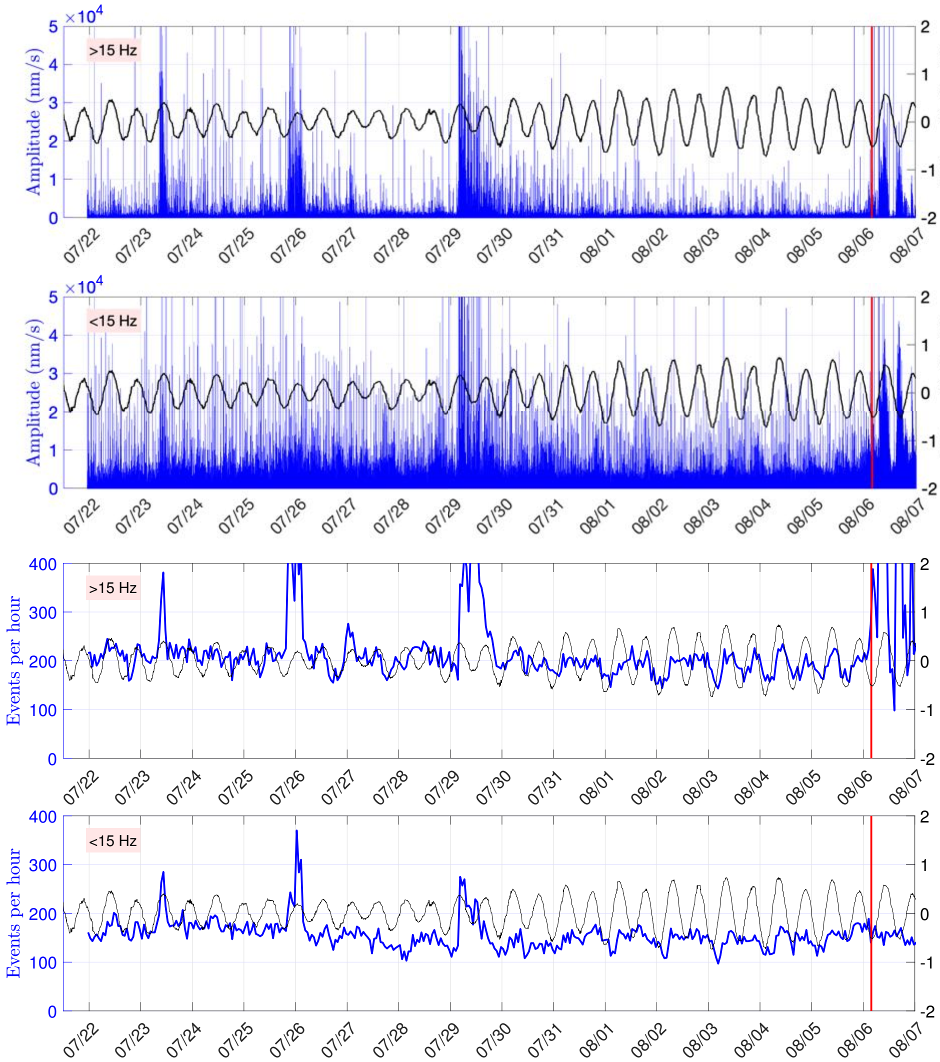

Figure 6: Seismic amplitude and number of STA/LTA detections (per hour) for different frequency bands as compared with tidal rates (–dz/dt), which were observed in Pituffik (Thule), 125 km away. Note that the tidal rates have the minus sign to help the eye. Red line marks the time of OBS release. The tidal rates were smoothed with a median filter that is 1.5 h long.

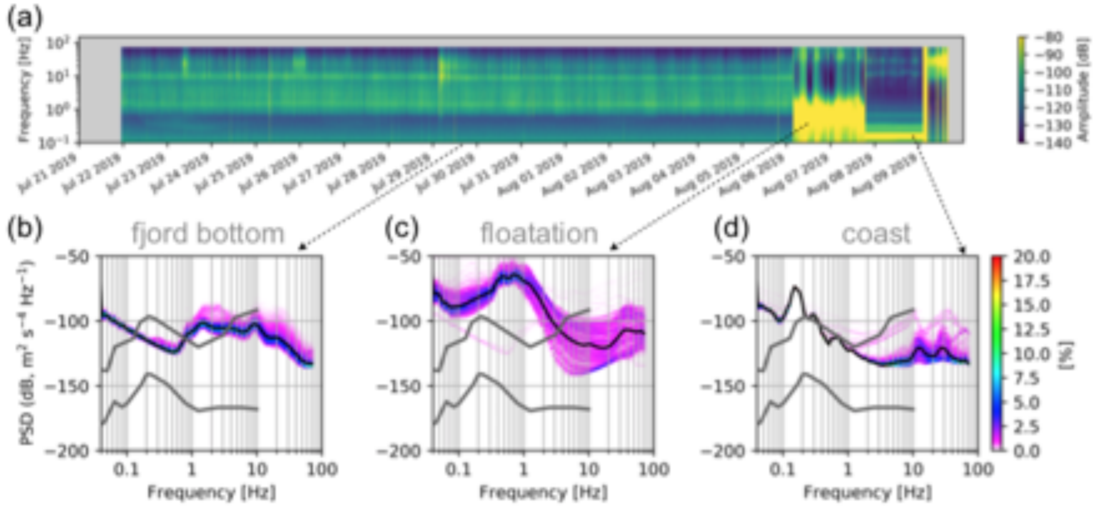

Figure 7: **(a)** Long-term spectrogram of continuous OBS data (vertical component for acceleration). **(b, c, d)** Corresponding PSD–PDFs for periods at the fjord seafloor (7278 segments), while floating (759 segments), and on the coast (599 segments). The median noise is indicated by the black curves. The data are compared with the standard Global Seismographic Network low- and high-noise models (grey curves; (McNamara and Buland, 2004)).

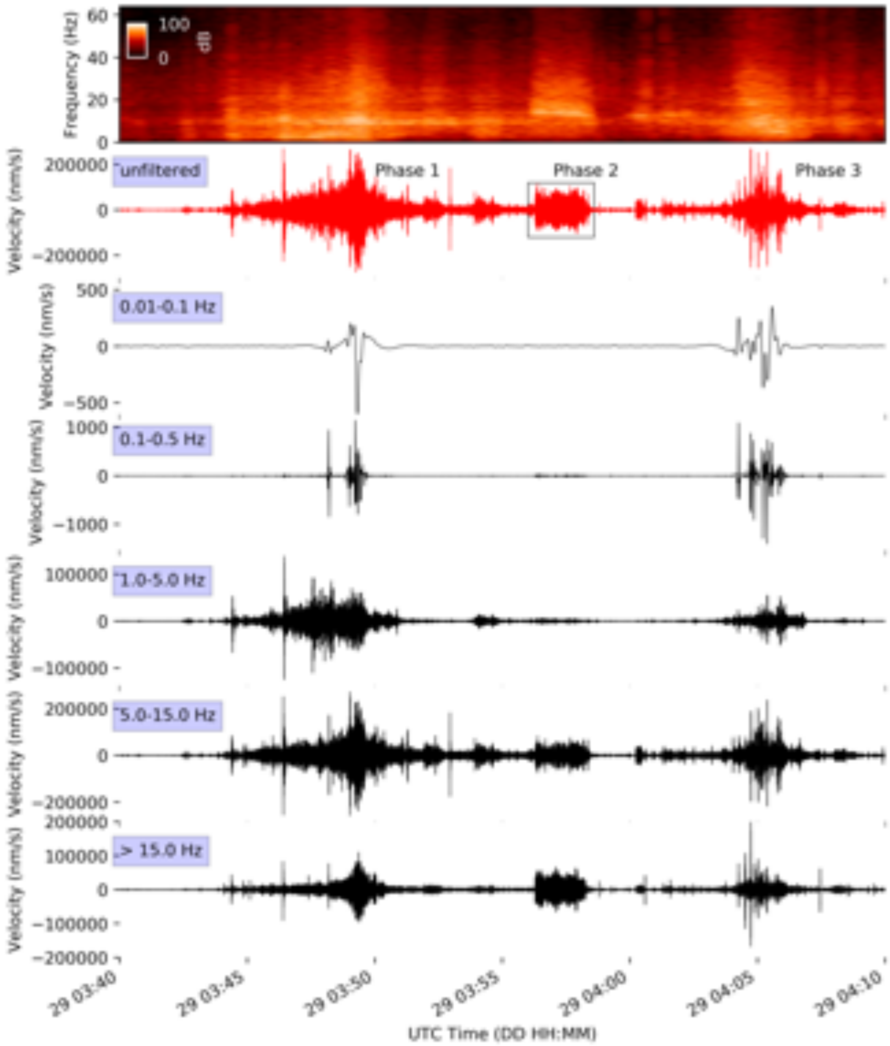

Figure 8: Spectrogram and decomposition of 30-min-long OBS waveforms during the major calving event (July 29, 2019) as different frequency bands. The Butterworth zero-phase shift filter with four corners was applied.

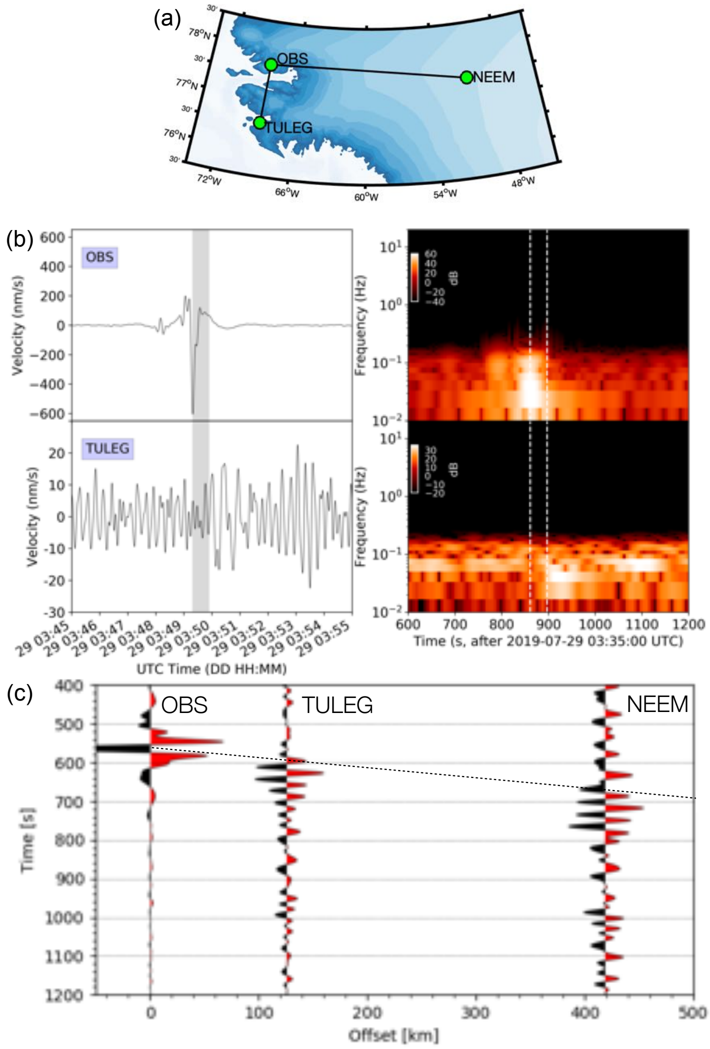

Figure 9: **(a)** Locations of the OBS (i.e., the source), TULEG, and NEEM stations with the shortest distances from the source shown as lines. **(b)** Bandpass-filtered waveforms (0.01–0.1 Hz) during Phase 1 of calving on July 29 as observed by the OBS and TULEG stations, with corresponding spectrograms (PSD was computed using a 60-s-long sliding windows with 90% overlap). The gray bar indicates the expected travel time between the stations, assuming a surface wave velocity of $3.5\,\mathrm{km\,s^{-1}}$. Dashed lines over the spectrograms indicate the same timing as the gray bar (i.e., the largest amplitude recorded by the OBS and its expected arrival time at TULEG). **(c)** Propagation of waveforms (bandpass filtered at 0.01–0.05 Hz) from the source (the slope corresponds to $3.5\,\mathrm{km\,s^{-1}}$; time is relative to 03:40 UTC).

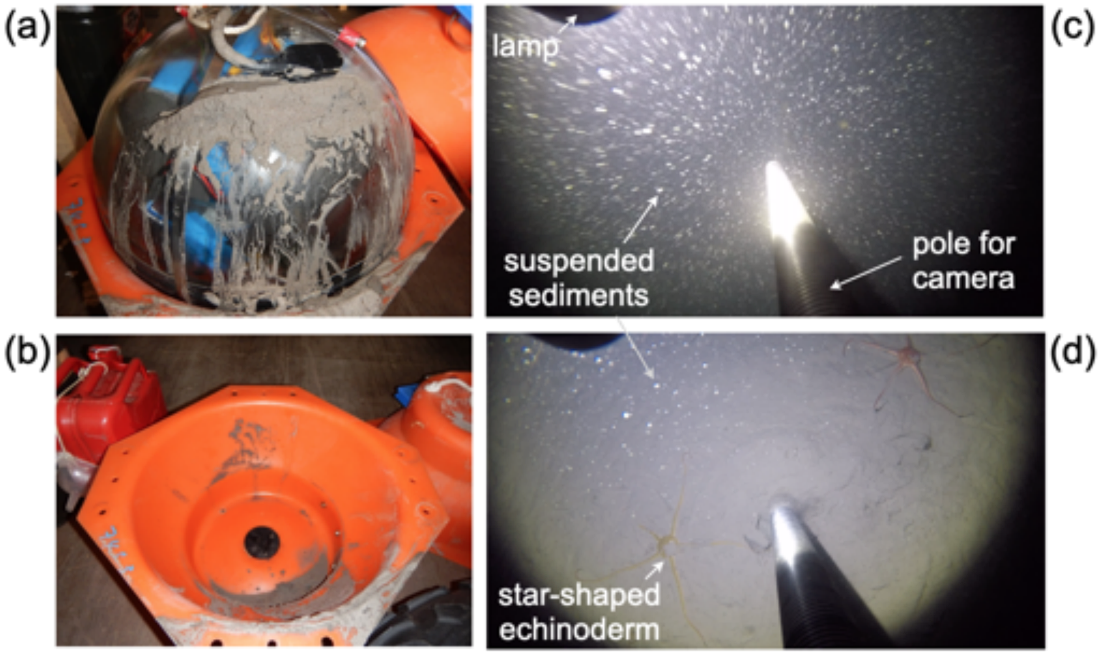

Figure 10: **(a, b)** Photographs of the OBS after retrieval and removal of the upper protective shell (credit: N. Kanna; August 2019). **(c, d)** Underwater photographs taken ~0.5 km from the OBS drop point and a few meters above and at the bottom of the fjord (200 m depth) during sediment coring of BF9 (diameter of the camera pole is 2.5 cm; credit: T. Ando; July 2018).

Appendix A (instrument response)

Additional characteristics of the seismic instrument were as follows. L-28LB 395 Ohm geophone had a nearly flat response between 4.5 and 300 Hz. Open-Circuit damping and sensitivity were 0.384 and 0.795, respectively. Response curve had two poles and two zeroes. The two complex poles were [–1.98e+01, 2.02e+01] and [–1.98e+01, –2.02e+01], respectively; both zeros were [0.0, 0.0].

Appendix B (Figures B1–B3)

Fig. B 1: A potentially useful methodology at the calving fronts: OBS deployment from a helicopter (offshore Hokkaido, Japan; credit: Y. Murai, February, 10, 2006). The shown OBS model is larger and slightly different in design from the one used in this study.

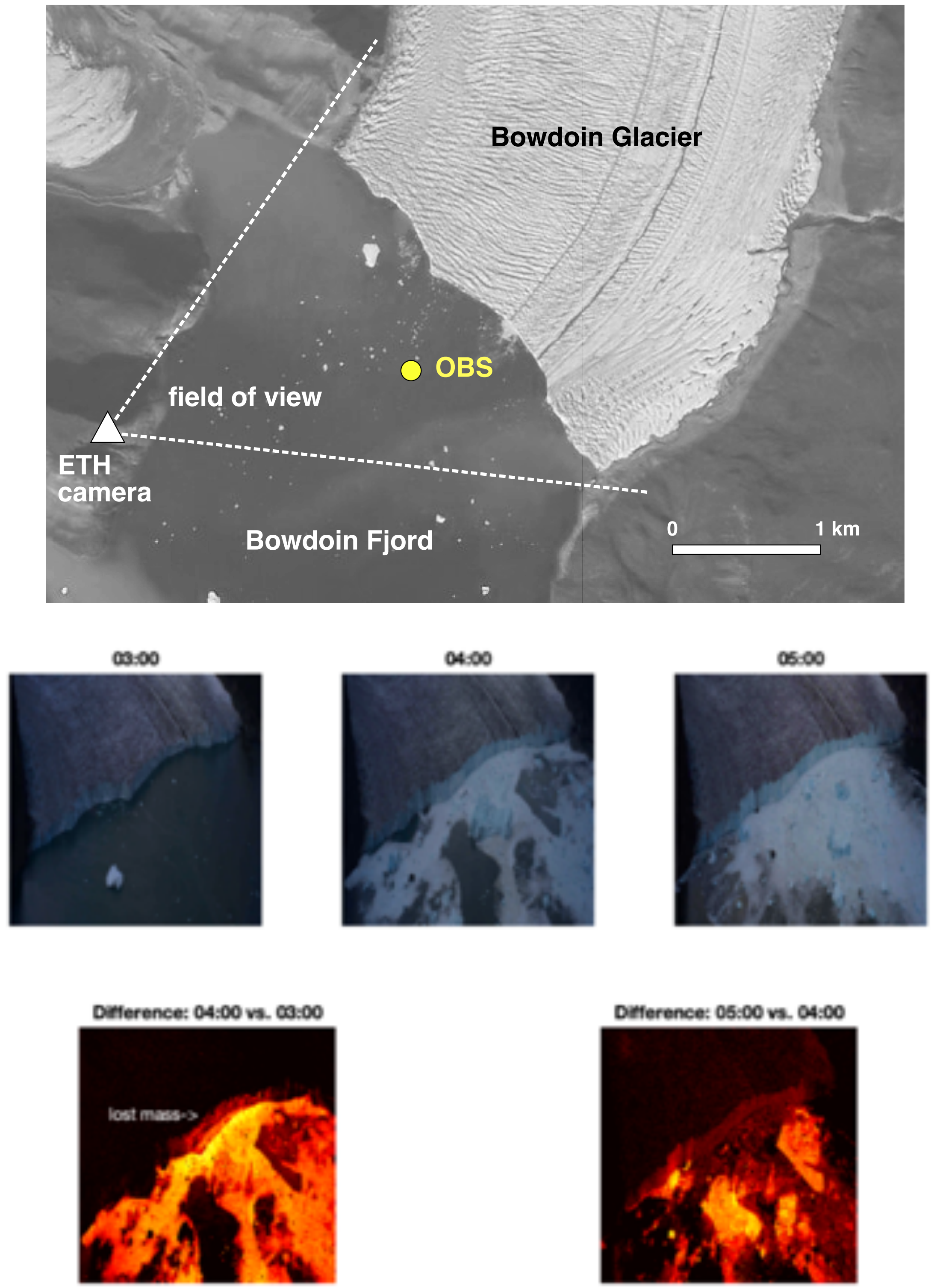

Fig. B 2: Map and hourly time-lapse images of the calving front and their differences, highlighting changes along the calving front (direct subtraction of the gray-scale intensity). Photographs were automatically taken from the same position as Fig. 2c (Sentinel Nunatak) on July 29, 2019, between 03:00 and 05:00 UTC (credit: E. van Dongen). Image distortion is due to the square cropping box. Satellite imagery was taken two days before the calving by Copernicus SENTINEL-2A, 27 July 2019.

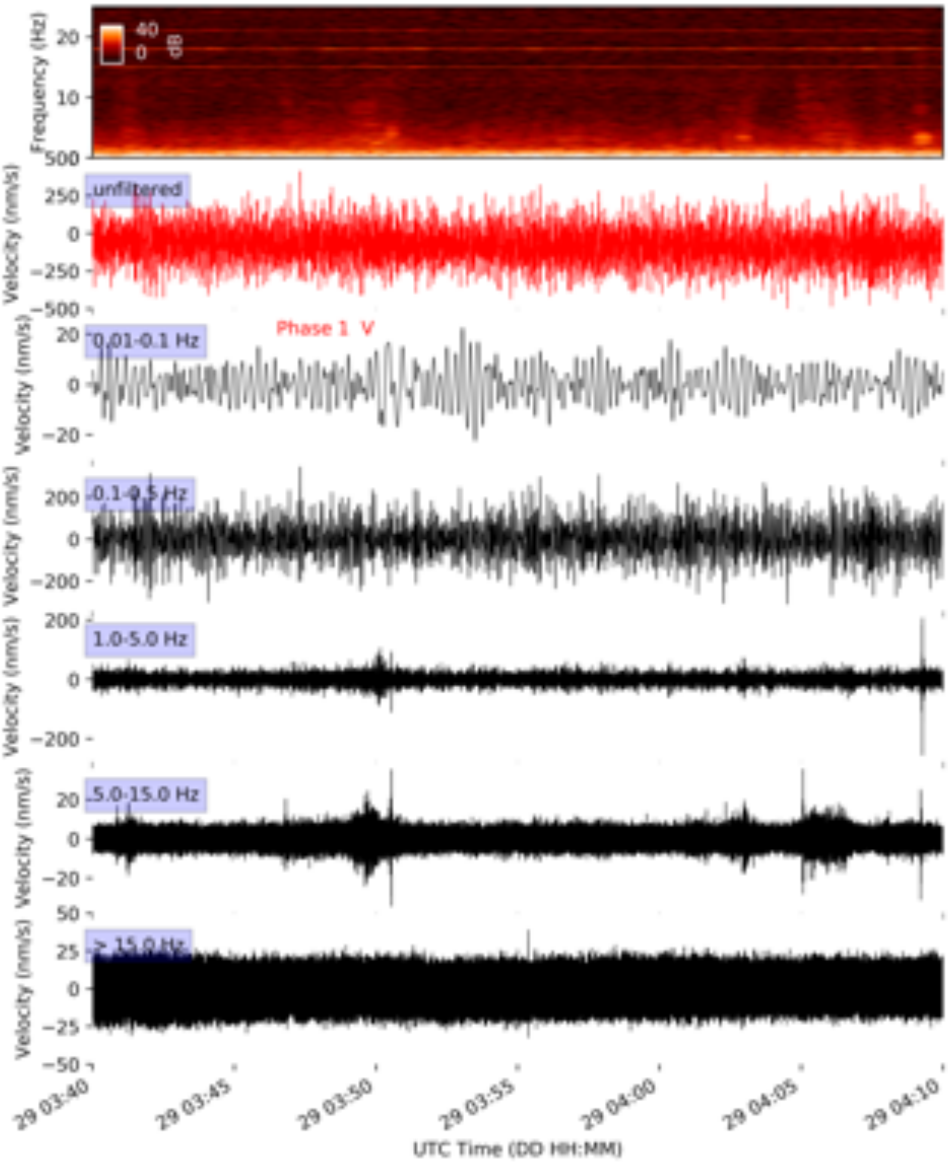

Fig. B 3: Spectrogram and decomposition of 30-min-long TULEG waveforms during the major calving event (July 29, 2019) in different frequency ranges. The Butterworth zero-phase shift filter with four corners was applied.